Numerical Heat Transfer, Part A, 52: 441–461, 2007

ISSN: 1040-7782 print/1521-0634 online
DOI: 10.1080/10407780701298585

Taylor & Francis
Taylor & Francis Group

FINITE-VOLUME METHODS FOR ISOTACHOPHORETIC SEPARATION IN MICROCHANNELS

Jaesool Shim and Prashanta Dutta
School of Mechanical and Materials Engineering, Washington State University, Pullman, Washington, USA

Cornelius F. Ivory
School of Chemical and Bioengineering, Washington State University, Pullman, Washington, USA

Numerical simulation results are obtained for isotachophoresis (ITP) in two-dimensional (2-D) straight microchannels. This 2-D ITP model is formulated based on finite-volume schemes using five ionic components: one leader, one terminator, two samples, and a counter-ion electrolyte. Distinct mobilities and diffusion coefficients are assigned to all ionic components, and an electric field is maintained along the channel to carry out the electrophoretic separation in the microchannel. The computer model is developed to solve the mass and charge conservation equations and to satisfy electroneutrality condition in the system. Three different finite-volume schemes, power-law, hybrid, and upwind, are tested to obtain the best numerical solution of this nonlinear electrophoretic problem. The normalized standard deviation technique is introduced to evaluate the performance of these three schemes. Numerical results show that the power-law scheme performs better; grid Peclet numbers up to 23 are acceptable for this nonlinear isotachophoresis. The effects of the applied electric potential, ionic mobilities and initial distribution of samples on the separation behavior are also presented.

1. INTRODUCTION

Isotachophoresis (ITP) is a separation and concentration technique used to isolate charged molecules or particles under the influence of an electric field. In ITP, a mixture of sample (target and/or impurities) ions is placed between a leading electrolyte and a terminating electrolyte. The electrophoretic mobilities, electrophoretic velocities per unit electric field, of sample ions are higher than that of a terminating ion and smaller than that of a leading ion, all with the same charge sizes. Hence, under the influence of external DC electric field, electrolytes separate and/or concentrate based on their net electrophoretic mobilities and form discrete zones. At steady state, the zone interfaces move at an "isotacho" or constant velocity. ITP can be used to boost throughput in preparative electrophoresis, and it can concentrate proteins to more than 10 mg/mL. It has the advantage over isoelectric focusing in that it

Received 21 October 2006; accepted 26 January 2007.
This investigation was supported in part by the Washington State University Office of Research and in part by the National Science Foundation under Grant CTS0300802.
Address correspondence to Prashanta Dutta, School of Mechanical and Materials Engineering, Washington State University, Pullman, WA 99164-2920, USA. E-mail: dutta@mail.wsu.edu

NOMENCLATURE

A	sample (electrolyte) A	t	time
B	sample (electrolyte) B	T	absolute temperature
C	concentration of electrolytes	TE	terminator or terminating electrolyte
D	diffusion coefficient	TP	total number of grid points
$\vec{E}$	electric field, $(= -\nabla\phi)$	$\vec{U}$	bulk flow velocity
F	Faraday constant $(= 96,484\text{C/mol})$	z	valence
$\vec{I}$	electric current density	Δx	grid size in x direction
LE	leader or leading electrolyte	Δy	grid size in y direction
M	total number of ionic species or electrolytes	ε	relative permittivity of medium
		ε_o	permittivity of free space $(= 8.85 \times 10^{-12}\text{C/Vm})$
$\vec{N}$	net flux of species		
NSD	normalized standard deviation	μ	electrophoretic mobility
Pe	cell Peclet number	ρ	charge density
$\vec{n}$	unit normal	σ	conductivity
R	universal gas constant	ϕ	electric potential
R_i	reaction term	ω	absolute mobility

can be performed at virtually any pH without facing the problem of isoelectric precipitation [1]. ITP technique can be used to separate both high- and low-molecular-weight ionic components. Through an experimental study, Kendall and Crittenden first demonstrated ITP to separate rare earth metals [2]. Since then a number of experimental and theoretical works on ITP have appeared in the literature [3–8].

General mathematical formulations of ITP were first reported by Kohlrausch [5]. He analyzed isotachophoresis quantitatively by introducing the concept of a regulating function which can define the conditions at the interface between two different ions with the same counter ion. Boček et al. [6] described separation capacity of ITP by developing a relationship between the amount and composition of a binary mixture and the amount of electricity that has to be passed through the system to obtain complete separation. In 1979, Mikkers et al. [7] introduced the concept of separation efficiency and resolution for ITP. The following year, Gebauer et al. [8] presented an experimental and theoretical work on ITP behavior of anionic complexes.

Until the early 1980s, most of the ITP literature was based on experimental and/or simplified theoretical models. Due to the complex nature of the ITP phenomena, it was not possible to obtain a complete analytical relationship of ITP even for a one-dimensional problem. In 1983, Bier et al. [9] proposed a full-scale, unified mathematical model for transient electrophoretic separation processes and presented simulation results for zone electrophoresis, moving-boundary electrophoresis, isotachophoresis and isoelectric focusing in a circular tube. Later, Fidler et al. [10] described a simplified mathematical model for ITP and obtained simulation results to separate two samples in a capillary tube. In their computer model, diffusion coefficients were ignored to simplify the computational effort. In the meantime, Mosher et al. described a computer model that takes care of diffusional effects for the exact prediction of boundary shape for weak electrolytes [11]. They also considered the pH effects in the computer model by including hydronium and hydroxyl ions in ITP. Heinrich and Wagner [12] developed an algorithm for robust simulation and optimization of electrophoretic processes using a one-dimensional transient-state

dynamic model. The effects of co- and counterflow on ITP transport behavior were predicted by Deshmukh and Bier [13]. They also verified their predictions with experimental results obtained from a large-scale recycling ITP apparatus. Šlais [14] presented the principle and theoretical model of ITP in a tapered capillary, and a relationship among channel shape, electrophoretic mobilities, and selectivity was proposed. Hirokawa et al. [15] used transient ITP as an on-line preconcentration method for capillary zone electrophoresis. More recently, a mathematical model was presented for any number of multivalent electrolytes in free solution [16].

Recently, on-chip isotachophoresis has received significant research attention due to its speed, cost-effectiveness, and low reagent consumption [17 and references therein]. Moreover, microchannel ITP is carried out in free solution rather than in a gel. Hence, this process can handle molecular weights ranging from peptides to large protein complexes or even organelles and whole cells. However, until today, there has been no two-dimensional numerical model for microchannel ITP. In this study, a 2-D (spatial) computer model is developed to simulate ITP in a microfluidic channel. To our knowledge this is the first 2-D ITP work developed for microchannels using finite-volume methods. Four different finite-volume schemes are presented for 2-D transient isotachophoresis. The effectiveness of different finite-volume schemes is studied to demonstrate the potential usefulness of these techniques.

2. ISOTACHOPHORESIS: THEORY AND GOVERNING EQUATIONS

Isotachophoresis is one of the four major electrophoretic techniques used to purify or isolate charged particles or solutes. It provides a more systematic and advanced separation technique than zone electrophoresis (ZE) or moving-boundary electrophoresis (MBE). This technique is also known as displacement electrophoresis, omegaphoresis, or transphoresis [11]. ITP is carried out between two homogeneous electrolyte solutions, a leader and a terminator, under the action of an electric field. The samples, which are generally a mixture of ionic components, are placed between the leader and the terminator. The electrophoretic mobility of the leader is higher, while the electrophoretic mobility of the terminator is lower. The electrophoretic mobility of the sample ions should be less than that of a leader and greater than that of a terminator. In order to have an effective separation, the net mobilities of sample ions should be distinct. On the other hand, ITP cannot be used to separate samples if the mobilities of the sample electrolytes are very close to each other.

Figure 1 shows a schematic of a cationic ITP process in a straight channel. In this case, the system consists of five ionic components: one leading electrolyte (LE), one terminating electrolyte (TE), two samples (samples A and B), and one counterion for satisfying electroneutrality condition in the system. At the initial time t_0, sample electrolytes (samples A and B) are placed between a leading electrolyte and a terminating electrolyte. Once the electric field is turned on ($t > t_0$), all cations will start moving toward the cathode, while the counterions (anions) will migrate toward the anode. Due to the distinct mobilities of electrolytes ($|\mu_T| < |\mu_B| < |\mu_A| < |\mu_L|$), the electrophoretic velocities of the leader, terminator, and sample electrolytes should be different. This fact will contribute to gradual separation of sample A from sample B with time. For instance, at time t_1 the overlapping regions of samples A

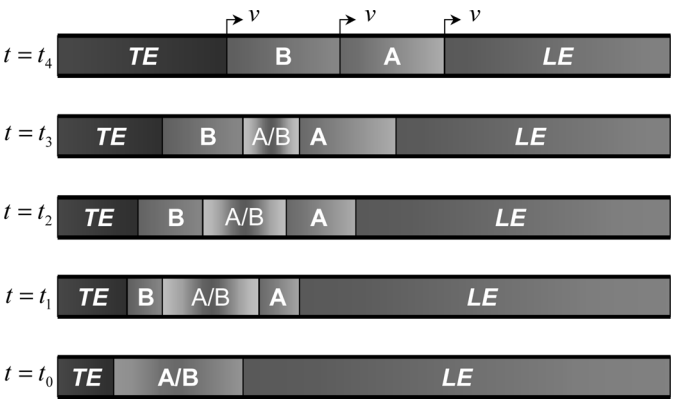

Figure 1. The isotachophoresis process with two samples, A and B. TE stands for the terminating electrolyte or terminator and LE denotes leading electrolyte or leader.

and B are much longer than that at time t_3. At time t_4, sample A is almost separated from sample B. Unlike isoelectric focusing, ITP cannot provide baseline separated peaks or zones. In other words, in ITP there will be little overlapping region between two adjacent zones. After reaching steady state ($t > t_4$), all three interfaces move with the same speed (v).

2.1. Mathematical Model

The modeling of ITP is based on migration of a set of ionized electrolytes of different mobilities toward the opposite electrode. The transport equation of the charged particles is given as

$$\frac{\partial C_i}{\partial t} + \nabla \cdot \vec{N}_i = R_i \tag{1}$$

where C_i is the concentration of the ith component of the electrolyte and R_i is the rate of generation of the ith component. The net flux, N_i, of the ith component can be expressed as

$$\vec{N}_i = -D_i \nabla C_i + (\mu_i \vec{E} + \vec{U}) C_i \tag{2}$$

where D_i and μ_i are the diffusion coefficient and net mobility of the ith charged component, respectively, $\vec{U}$ is the applied velocity field in the system, and $\vec{E}$ is the electric field. The electrophoretic mobility of a component (μ_i) can be defined as the product of the valence (z_i) and the absolute mobility (ω_i). The rate of generation of ith component is assumed to be negligible, and the mass conservation equation of the ith species can be rewritten as

$$\frac{\partial C_i}{\partial t} + \nabla \cdot \vec{N}_i = \frac{\partial C_i}{\partial t} + \nabla \cdot \left[-D_i \nabla C_i + (z_i \omega_i \vec{E} + \vec{U}) C_i \right] = 0 \tag{3}$$

The multiplication of Eq. (3) by the Faraday constant (F) and z_i and the summation of all charged species allows us to arrive at the charge conservation equation

$$\frac{\partial \rho}{\partial t} + \nabla \cdot \vec{I} = 0 \tag{4}$$

where charge density (ρ) and electric current density (I) are defined as

$$\rho = F \sum_{i=\text{all}} z_i C_i \tag{5}$$

$$\vec{I} = F \sum_{i=\text{all}} z_i \vec{N}_i \tag{6}$$

The charge density is related to the electric potential by the Poisson equation as

$$\rho = F \sum_{i=\text{all}} z_i C_i = \varepsilon \varepsilon_0 \nabla \cdot \vec{E} \tag{7}$$

where ε is the relative permittivity of the medium and $\varepsilon_o = 8.85 \times 10^{-12}\,\text{C/Vm}$ is the permittivity of free space. In a microfluidic chip, the contribution of $\left(\varepsilon \varepsilon_o \nabla \cdot \vec{E}\right)/F$ can be neglected, and Eq. (7) can be rewritten as

$$\sum_{i=\text{all}} z_i C_i = 0 \tag{8}$$

Equation (8) represents the electroneutrality in the system. Note that the right-hand side of Eq. (7) cannot be neglected in nanochannel electrophoresis. Following Eqs. (4)–(8), one can rewrite the modified charge conservation as

$$\nabla \cdot \vec{I} = \nabla \cdot \left\{ \sigma \vec{E} - F \left[\sum_{i=1}^{M} D_i z_i \nabla C_i - \vec{U}_i (z_i C_i) \right] \right\} = 0 \tag{9}$$

where M is the total number of ionic species. The ionic conductivity can be given as

$$\sigma = F \left(\sum_{i=1}^{M} z_i^2 \omega_i C_i \right) \tag{10}$$

The above governing equations are valid based on the following assumptions and approximations.

1. The ionic association and dissociation effects of each species are neglected.
2. Joule heating is not considered; i.e., temperature is assumed constant throughout the channel. This can be justified in a microfluidic system due to the large surface-to-volume ratio.
3. Fluid properties such as the diffusion constant and permittivity are assumed uniform throughout the channel. For low-electric-field applications, the variations of mobilities and diffusion coefficients are negligible.
4. The effects of pH are not considered in this model. The concentrations of hydronium and hydroxyl ions are generally negligible compared to the concentrations of the species to be separated.

2.2. Computational Model

In this model, one leader, one terminator, two sample electrolytes, and one counterelectrolyte are used for isotachophoretic separation. The concentrations of charged ions (leader, terminator, and samples) are obtained from the species transport (mass conservation) equation. In solving the mass conservation equation, no electroosmotic flow is taken into account in this model [18]. The diffusion coefficient (D_i) of each species is calculated from the absolute mobility (ω_i) using the Nernst-Einstein equation as

$$D_i = \frac{RT\omega_i}{F} \tag{11}$$

where R is the universal gas constant and T is the absolute temperature. The concentration of the counterions is calculated from the electroneutrality equation [Eq. (8)].

The electric field $\left(\vec{E} = -\nabla\phi\right)$ can be obtained from the modified charge conservation equation. Hence, in the absence of any bulk flow, the modified charge conservation equation can be simplified to

$$\nabla \cdot (\sigma \nabla \phi) = -\nabla . \left(F \sum_{i=1}^{M} D_i z_i \nabla C_i \right) \tag{12}$$

The contribution of the right-hand side is very negligible at all locations, except at the interfaces of any two components, where electrolyte concentration generally changes abruptly. In the numerical computation, the electric potential (ϕ) is calculated from Eq. (12).

2.3. Initial and Boundary Conditions

ITP simulation is strongly dependent on the initial distribution of all charged species. In this study it is assumed that the leader, terminator, and the two samples are initially distributed along the channel in an arbitrary fashion. In solving mass conservation equations, the net flux through the channel walls and end wells (reservoirs) are set to zero. The electric potential is subject to insulating boundary conditions ($\nabla\phi \cdot \vec{n} = 0$) on the walls, and constant potentials are maintained at the electrode (end) wells. In this study, the electric potential at the anodic (terminator) well is varied from case to case, while the potential at the cathodic (leader) well is maintained at ground ($\phi_L = 0$).

3. NUMERICAL SCHEME

It is difficult or sometimes impossible, even for the one-dimensional case, to solve analytically the set of ITP differential equations described earlier. In the past, a variety of numerical schemes or algorithms have been implemented for one-dimensional ITP problems. Thormann and Mosher have solved the 1-D differential equations by using DARE-P based software [19]. Fidler et al. have utilized universal control subroutines (SYMHYB) in Fortran-based language for 1-D simulation [10]. Recently, Hruška et al. solved the nonlinear partial differential equations using Simul 5, a free dynamic simulator [16]. However, these works addressed only one-dimensional computational geometries. In this work, 2-D finite-volume methods are developed to solve the mass and charge conservation given by Eqs. (3) and (12).

Finite-volume methods are popularly used in solving mass, momentum, and energy equations for electrokinetic microflow [20], natural convection [21], laser surface processing [22], phase-change processes [23], etc. In finite-volume methods, algebraic equations are obtained for each dependent variable at each grid point by performing volume integral across the finite computational domain. The primary advantage of finite-volume methods is that the resulting solutions satisfy the conservation of mass, momentum, and energy at each grid face as well as for the whole computational domain. Unlike spectral element methods [24], these techniques can handle sharp boundaries without any major grid refinement. Moreover, they can easily be adapted for complex and irregular geometry. In this study, finite-volume techniques are developed for electromigration diffusion-type problems such as ITP, isoelectric focusing [25], etc.

3.1. Discretized Equations

The mass conservation equation can be written in two-dimensional form as

$$\frac{\partial C_i}{\partial t} + \frac{\partial[-D_i(\partial C_i/\partial x) + (\mu_i E_x)C_i]}{\partial x} + \frac{\partial\left[-D_i(\partial C_i/\partial y) + \left(\mu_i E_y\right)C_i\right]}{\partial y} = 0 \qquad (13)$$

where E_x and E_y are the electric field in the x and y directions, respectively. Now, integration of Eq. (13) over the two-dimensional control volume shown in Figure 2

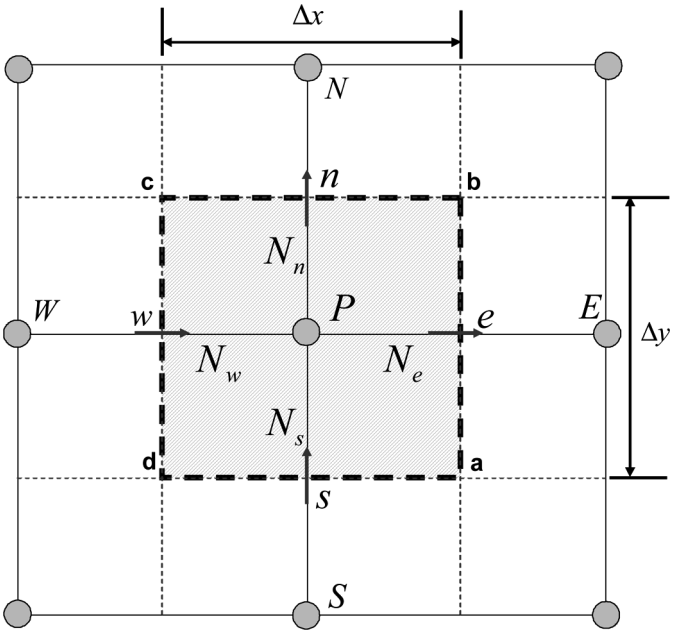

Figure 2. Schematic of a 2-D control volume. Dashed line *abcd* represents the control surface. Points *E*, *W*, *N*, and *S* are the east, west, north, and south neighbors of control point *P*. The height in the *z* direction (perpendicular to the paper) is unit.

yields

$$(C_i - C_i^o)_P \frac{\Delta x\,\Delta y}{\Delta t} + [(\mu_i E_x) C_i]_e \Delta y - [(\mu_i E_x) C_i]_w \Delta y + [(\mu_i E_y) C_i]_n \Delta x - [(\mu_i E_y) C_i]_s \Delta x$$
$$= \left(D_i \frac{\partial C}{\partial x}\right)_e \Delta y - \left(D_i \frac{\partial C}{\partial x}\right)_w \Delta y + \left(D_i \frac{\partial C}{\partial y}\right)_n \Delta x - \left(D_i \frac{\partial C}{\partial y}\right)_s \Delta x \tag{14}$$

The superscript o represents the old value (the value at the previous time step). The concentration of any component (i) at an interface can be found using linear interpolation of nodal values, while central differencing technique can be used for the spatial derivatives at the interface. Therefore, Eq. (14) can be expressed as (omitting subscript i)

$$\frac{\Delta x\,\Delta y}{\Delta t} C_P - \frac{\Delta x\,\Delta y}{\Delta t} C_P^0 + \frac{1}{2}(\mu E_x)_e \Delta y (C_E + C_p)$$
$$- \frac{1}{2}(\mu E_x)_w \Delta y (C_P + C_W) + \frac{1}{2}(\mu E_y)_n \Delta x (C_N + C_p) - \frac{1}{2}(\mu E_y)_s \Delta x (C_P + C_S)$$
$$= \frac{D_e}{\Delta x} \Delta y (C_E - C_P) - \frac{D_w}{\Delta x} \Delta y (C_P - C_W) + \frac{D_n}{\Delta y} \Delta x (C_N - C_P) - \frac{D_s}{\Delta y} \Delta x (C_P - C_N) \tag{15}$$

Therefore, the 2-D discretized equation becomes

$$a_P C_P = a_E C_E + a_W C_W + a_N C_N + a_S C_S + a_P^0 C_p^0 \tag{16}$$

where

$$a_E = \frac{D_e}{\Delta x} \Delta y - \frac{1}{2}(\mu E_x)_e \Delta y = G_e - \frac{1}{2} F_e = G_e (1 - 0.5|P_e|) + [[0, -F_e]] \tag{17a}$$

$$a_W = \frac{D_w}{\Delta x} \Delta y + \frac{1}{2}(\mu E_x)_w \Delta y = G_w + \frac{1}{2} F_w = G_w (1 - 0.5|P_w|) + [[0, F_w]] \tag{17b}$$

$$a_N = \frac{D_n}{\Delta y} \Delta x - \frac{1}{2}(\mu E_y)_n \Delta x = G_n - \frac{1}{2} F_n = G_n (1 - 0.5|P_n|) + [[0, -F_n]] \tag{17c}$$

$$a_S = \frac{D_s}{\Delta y} \Delta x + \frac{1}{2}(\mu E_y)_s \Delta x = G_s + \frac{1}{2} F_s = G_s (1 - 0.5|P_s|) + [[0, F_s]] \tag{17d}$$

$$a_P^0 = \frac{\Delta x\,\Delta y}{\Delta t} \tag{17e}$$

$$a_P = a_E + a_W + a_N + a_S + a_P^0 + (F_e - F_w) + (F_n - F_s) \tag{17f}$$

Table 1. Coefficients of discretized algebraic equations [Eqs. (17*a*)–(17*e*)] for different finite-volume schemes [26]

	Upwind	Hybrid	Power law
a_E	$G_e + [[0, -F_e]]$	$G_e[[0, 1 - 0.5\lvert P_e\rvert]] + [[0, -F_e]]$	$G_e[[0, (1 - 0.5\lvert P_e\rvert)^5]] + [[0, -F_e]]$
a_W	$G_w + [[0, F_w]]$	$G_w[[0, 1 - 0.5\lvert P_w\rvert]] + [[0, F_w]]$	$G_w[[0, (1 - 0.5\lvert P_w\rvert)^5]] + [[0, F_w]]$
a_N	$G_n + [[0, -F_n]]$	$G_n[[0, 1 - 0.5\lvert P_n\rvert]] + [[0, -F_n]]$	$G_n[[0, (1 - 0.5\lvert P_n\rvert)^5]] + [[0, -F_n]]$
a_S	$G_s + [[0, F_s]]$	$G_s[[0, 1 - 0.5\lvert P_s\rvert]] + [[0, F_s]]$	$G_s[[0, (1 - 0.5\lvert P_s\rvert)^5]] + [[0, F_s]]$
a_P^0	$\frac{\Delta x\,\Delta y}{\Delta t}$	$\frac{\Delta x\,\Delta y}{\Delta t}$	$\frac{\Delta x\,\Delta y}{\Delta t}$

The electromigration strengths, diffusion strengths, and cell Peclet numbers can be defined as

$$F_e = (\mu E_x)_e \Delta y \quad F_w = (\mu E_x)_w \Delta y \quad F_n = (\mu E_y)_n \Delta x \quad F_s = (\mu E_y)_s \Delta x$$

$$G_e = \frac{\Delta y}{\Delta x} D_e \quad G_w = \frac{\Delta y}{\Delta x} D_w \quad G_n = \frac{\Delta x}{\Delta y} D_n \quad G_s = \frac{\Delta x}{\Delta y} D_s$$

$$P_e = \frac{F_e}{G_e} \quad P_w = \frac{F_w}{G_w} \quad P_n = \frac{F_n}{G_n} \quad P_s = \frac{F_s}{G_s}$$

Using an identical procedure one can find the discretized equations of the mass conservation equation for other finite-volume schemes such as upwind, hybrid, or power-law. In finite-volume schemes, the general format of the discretized equations should be the same as Eq. (16) [26], but the coefficients will be different for different schemes. Following the method described in [26], the coefficients for different finite-volume schemes are presented in Table 1.

The discretized algebraic equations are obtained at each grid point for the mass conservation and modified charge conservation equations. For computational simplicity and stability, structured grids are considered in the simulation. The tridiagonal matrix algorithm (TDMA) is used to solve the discretized algebraic equations along a grid line, and line-by-line iteration is employed until converged results are obtained throughout the computational domain. The convergence criteria are set as $|(C_n - C_{n-1})/C_n| \leq 10^{-5}$ and $|(\phi_n - \phi_{n-1})/\phi_n| \leq 10^{-5}$ for the mass conservation and charge conservation equations, respectively. The subscripts n and $n-1$ denote the current and previous iteration step.

4. RESULTS AND DISCUSSION

ITP simulations are performed in a planar microchannel for five ionic components. Potassium ions [K^+] and tetrabutylammonium ions [$(C_4H_9)_4N^+$] are used as leader and terminator, and sodium ions [Na^+] and tetraethylammonium ions [$(C_2H_5)_4N^+$] are used as samples A and B, respectively. The physicochemical properties of all electrolytes are presented in Table 2. For effective separation using ITP, the mobilities of samples A and B are less than that of the leader, but more than that of the terminator. Though the current model can easily be extended to separate three or more samples, two samples are considered here for simplicity. In this study, the effective valences of all components are set as unity throughout the separation process. However, using this model, it is possible to simulate an ITP case having different

Table 2. The physicochemical properties of different electrolytes used in the ITP simulation. The diffusion coefficients are calculated using Eq. (11). The absolute mobility of the leader is the highest, while the absolute mobility of the terminator is the least

Component	Valence	Absolute mobility (m^2/Vs)	Diffusion coefficient [m^2/s]
Counter ion [Cl^-]	−1	7.918E-08	2.047E-09
Leader [K^+]	1	7.518E-08	1.943E-09
Terminator [$(C_4H_9)_4N^+$]	1	1.980E-08	5.118E-09
Sample A [Na^+]	1	5.592E-08	1.445E-09
Sample B [$(C_2H_5)_4N^+$]	1	3.420E-08	8.840E-09

valences of electrolytes. Figure 3 shows the computational domain and the initial concentration distribution for a leader, samples A and B, and terminator. The initial shape of the sample electrolytes is assumed to be Gaussian-like, while both leader and terminator are assumed uniformly distributed in the left and right edge of the microchannel. In this study, the channel length and width are kept constant at 20 cm and 200 μm, respectively. The ITP separation is initiated by applying an electric field along the channel as shown in Figure 3.

4.1. Finite-Volume Schemes

Four well-known finite-volume schemes, central differencing, upwind, hybrid, and power-law, are developed and tested for this nonlinear unsteady electromigration-diffusion problem. An electric potential of 6,000 V is applied in the anodic side,

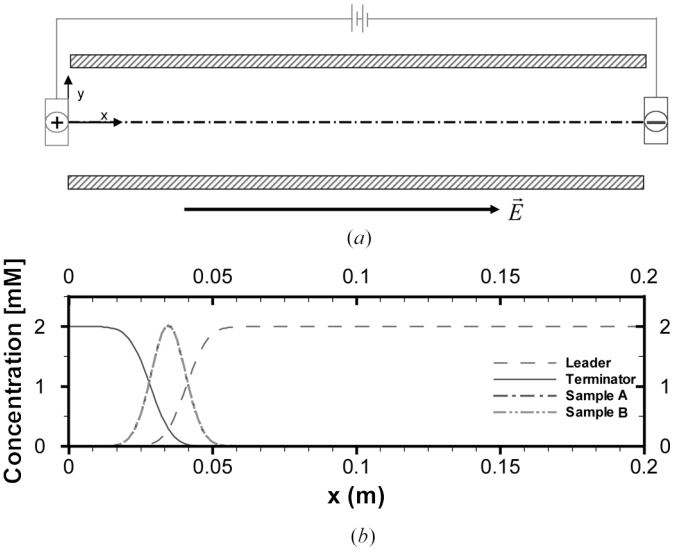

Figure 3. (*a*) Schematic view of computational domain for isotachophoresis in planar microchannel. The channel length is 20 cm and the channel width is 200 μm. In numerical simulation, a constant electric field is maintained by defining electric potentials at the anode and cathode. (*b*) Initial concentrations of system components for an ITP simulation.

while the cathodic side is connected to a ground (0 V). Figure 4 shows the predicted positions of electrolytes based on the upwind, hybrid, and power-law schemes. The numerical results of the central difference scheme are not presented here due to stability and convergence issues. Numerical results are extracted along the channel centerline at 40 s after the initiation of electric field. These results reveal that the power-law scheme (Figure 4*a*) is more effective in predicting ITP behavior than that of the hybrid or upwind scheme (Figures 4*b* and 4*c*). The power-law and hybrid schemes are able to create a discontinuous boundary between adjacent electrolytes, while the upwind scheme predicts significant overlapping regions between samples A and B. This is due to the fact that the upwind scheme is not able to handle a very sharp gradient without utilizing finer grid spacing. The effect of grid size is discussed in the next section.

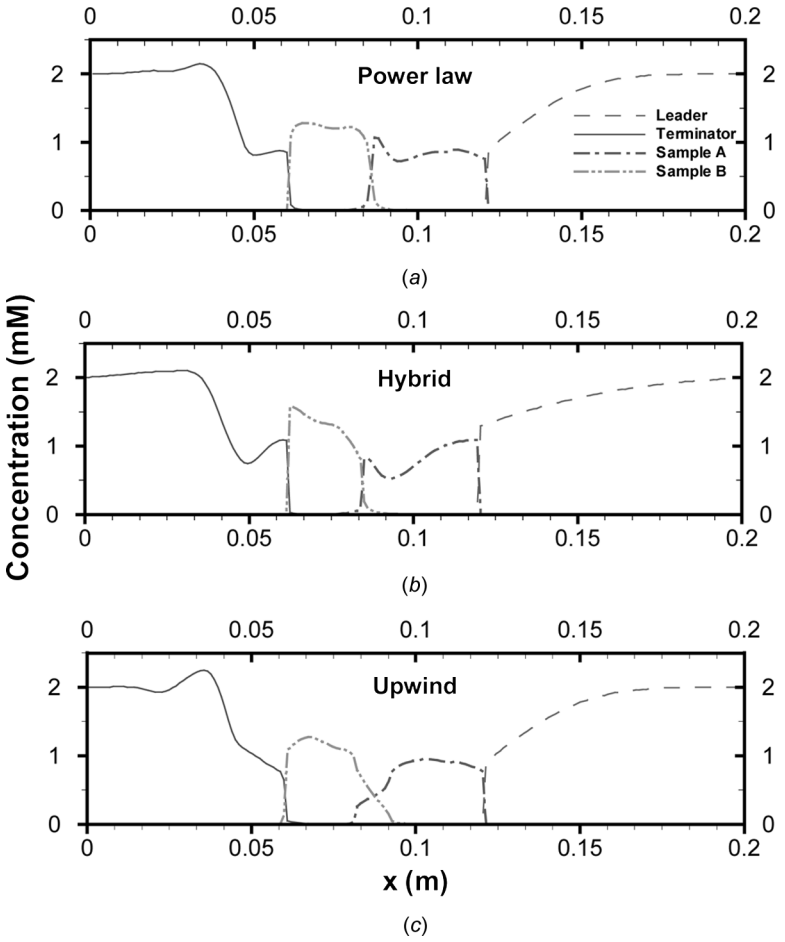

Figure 4. Isotachophoretic separation obtained at 40 s using (*a*) power-law scheme, (*b*) hybrid scheme, and (*c*) upwind scheme. The ITP simulation is carried out at a nominal electric field of 300 V/cm. The grid sizes are $\Delta x = 10\,\mu\text{m}$ and $\Delta y = 10\,\mu\text{m}$. The numerical results for the central difference scheme are not presented due to the stability problem.

Numerical results obtained from the power-law scheme agree qualitatively with the existing 1-D model [10], where initial concentration distribution was different from this study and a constant current density was used instead of constant electric potential. ITP separation is generally performed by maintaining constant potentials at the end reservoirs. The numerical results of Fidler et al. [10] show very sharp sample and leader bands, as they did not consider molecular diffusion effects. In this study the contribution of finite molecular diffusion is taken into consideration, and hence the electrolyte boundaries are not as sharp as predicted by Fidler et al. [10].

To compare the three different finite-volume schemes quantitatively, it is assumed that the samples proceed to the cathode with flat or uniform concentrations after producing discontinuous boundaries during separation process. The effectiveness of different techniques are determined by introducing a *normalized standard deviation* for an electrolyte as

$$\mathrm{NSD} = \left[\frac{1}{J}\sum_{k=1}^{\mathrm{TP}}\left(\frac{C_k m}{\frac{1}{J}\sum_{k=1}^{\mathrm{TP}} C_k m} - 1\right)\right]^{1/2} \quad \begin{array}{l} m = 1 \text{ if } C_k \neq 0 \\ m = 0 \text{ if } C_k = 0 \end{array} \tag{18}$$

where C_k is the concentration at any grid point k, J is the total number of grid points in the x direction having nonzero sample concentration, and TP is the total number of grid points in the x direction. The normalized standard deviation denotes a unified separation quality regardless of the initial concentration distribution in the system. Table 3 presents the normalized standard deviation (NSD) of samples A and B for three different finite-volume schemes. It is clear that, for samples A and B, the power-law scheme provides the least error in the band shape, while the upwind scheme offers the highest deviation from the ideal profile. Thus, the power-law scheme offers the best result for ITP simulations involving unsteady electromigration and diffusion terms.

The computational times needed by different finite-volume schemes are also presented in Table 3. An XP-based desktop computer (Dell, Pentium 4) was used to perform the ITP simulation in a 2-D channel for 40 s. The power-law scheme took longer time than the upwind and hybrid techniques. This is due to the fact that the coefficients of the power-law scheme are more complex than those of other two finite-volume techniques.

Table 3. The normalized standard deviation (NSD) of samples A and B for three different finite volume schemes. All conditions are same as Figure 4. The computer time is based on 40 s of computation in an XP-based desktop (Dell Pentium 4, 2 GB RAM, 3.4 GHz)

Numerical scheme	NSD (sample A)	NSD (sample B)	Computational time (h)
Power-law	0.0131	0.0671	216.8
Hybrid	0.0162	0.0839	195.4
Upwind	0.0168	0.0997	187.7

4.2. Grid Independence

To obtain numerically converged results, the effect of grid size is very important. For a numerical problem, it is easy to determine the appropriate grid size if an analytical solution is available for that problem. Since ITP is a nonlinear process, a closed-form analytical solution is not possible even for a very simple problem. Hence, we have to determine the appropriate grid size by increasing the number of grid points in the computational domain. In this study, we have considered a 2-D planar channel. Thus, the number of grid points in the x direction is varied, while the number of grids in the y direction is kept constant.

Numerical results are presented in Figure 5 for four different grid sizes ($\Delta x = 80, 40, 20$, and $10\,\mu$m). The initial concentration distributions for these cases are shown in Figure 3. The mobilities and diffusion coefficients of different electrolytes are presented in Table 2. The ITP simulations are performed for a nominal electric field of 300 V/cm, and the power-law scheme is used in this case.

In an electromigration-diffusion problem, the grid size can be related with the cell Peclet number as

$$\mathrm{Pe}_i = z_i \frac{\omega_i}{D_i} \frac{d\phi}{dx} \Delta x = \frac{F z_i}{RT} \frac{d\phi}{dx} \Delta x \tag{19}$$

For a particular electric field, the cell Peclet number is directly related to the grid size. In our study ($|z_i| = 1; F = 96,484\,\mathrm{C/mol}; R = 8.314\,\mathrm{J/mol\,K}; T = 303\,\mathrm{K}$), the cell Peclet numbers for Figures 5*a*, 5*b*, 5*c*, and 5*d* become 92, 46, 23, and 11.5, respectively. It is clear that at high grid Peclet number the numerical results do not converge. In all four cases, the discrete boundaries between leader and sample A and between terminator and sample B take place at the same location, but for higher grid Peclet numbers (Figures 5*a* and 5*b*) the overlapping region between samples A and B is different. Our numerical results show that converged results can be obtained for grid Peclet number 23 or less. Thus, for a power-law scheme, the total number of elements in the x direction is set to 10,000 for the rest of the article. It is important to note that the critical grid Peclet number for other numerical schemes such as central difference or upwind should be smaller than that of the power-law scheme. In other words, finer grids are needed if one would like to use upwind or central difference scheme for this nonlinear problem.

4.3. Transient Behavior of Electrolytes in ITP Process

Figure 6 illustrates the transient behavior of leader, terminator, and sample components (A and B) in a 2-D straight channel under a nominal electric field of 300 V/cm. The electrophoretic mobilities and diffusion coefficients of all electrolytes are presented in Table 2. In this case, the power-law scheme is used to form the discretized algebraic equations for the mass and charge conservation equations. To obtain grid-independent results, 10,001 grid points are considered in the x-direction and 21 grid points are used in the y direction. The initial concentration profiles of samples A and B are kept identical and Gaussian-like (Figure 6*a*). Simulation results show that all electrolytes (except counterions) start moving toward the cathode once

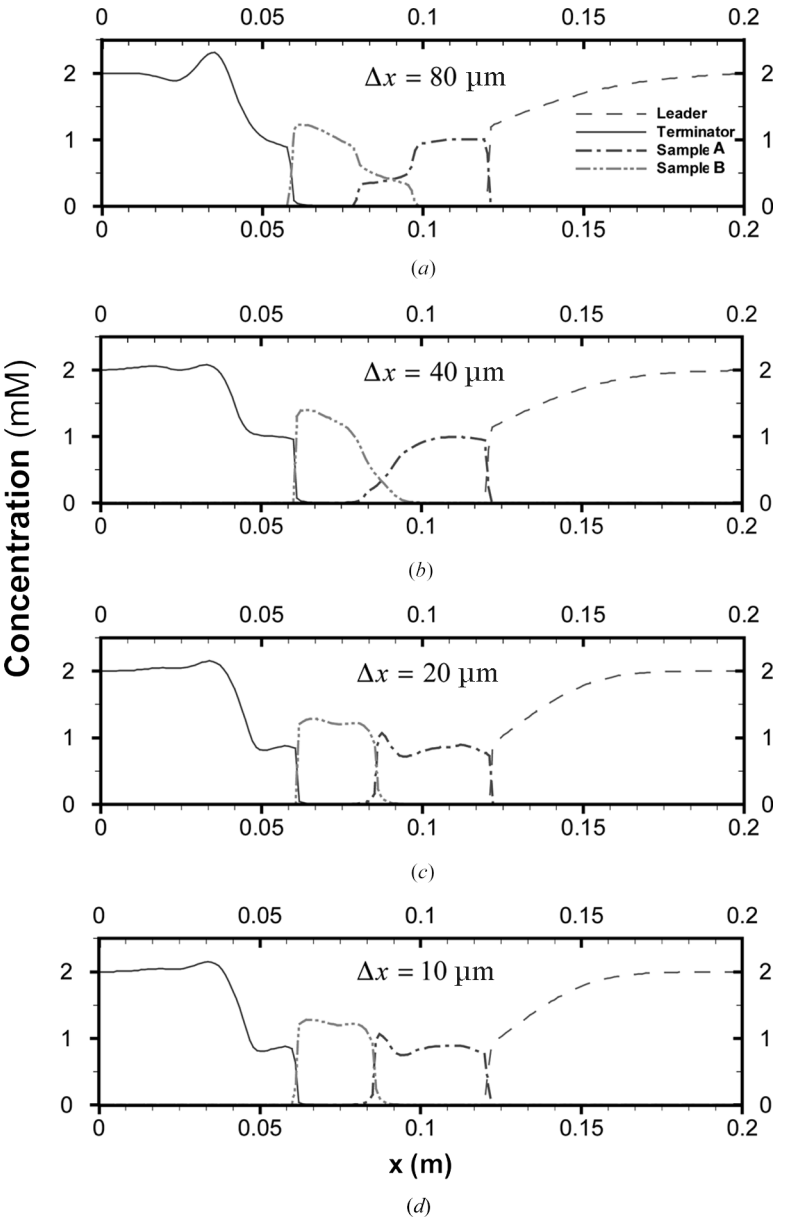

Figure 5. The effects of grid size on numerical prediction of ITP behavior. The cell Peclet numbers for cases (*a*), (*b*), (*c*), and (*d*) are 92, 46, 23, and 11.5, respectively.

an electric field is applied along the channel. At the beginning of the separation process, the leader moves at a faster pace than the samples or terminator, due to the higher electrophoretic mobility. The relative movement of each electrolyte is evident from the sample displacement. Due to the higher mobility, sample A starts separating

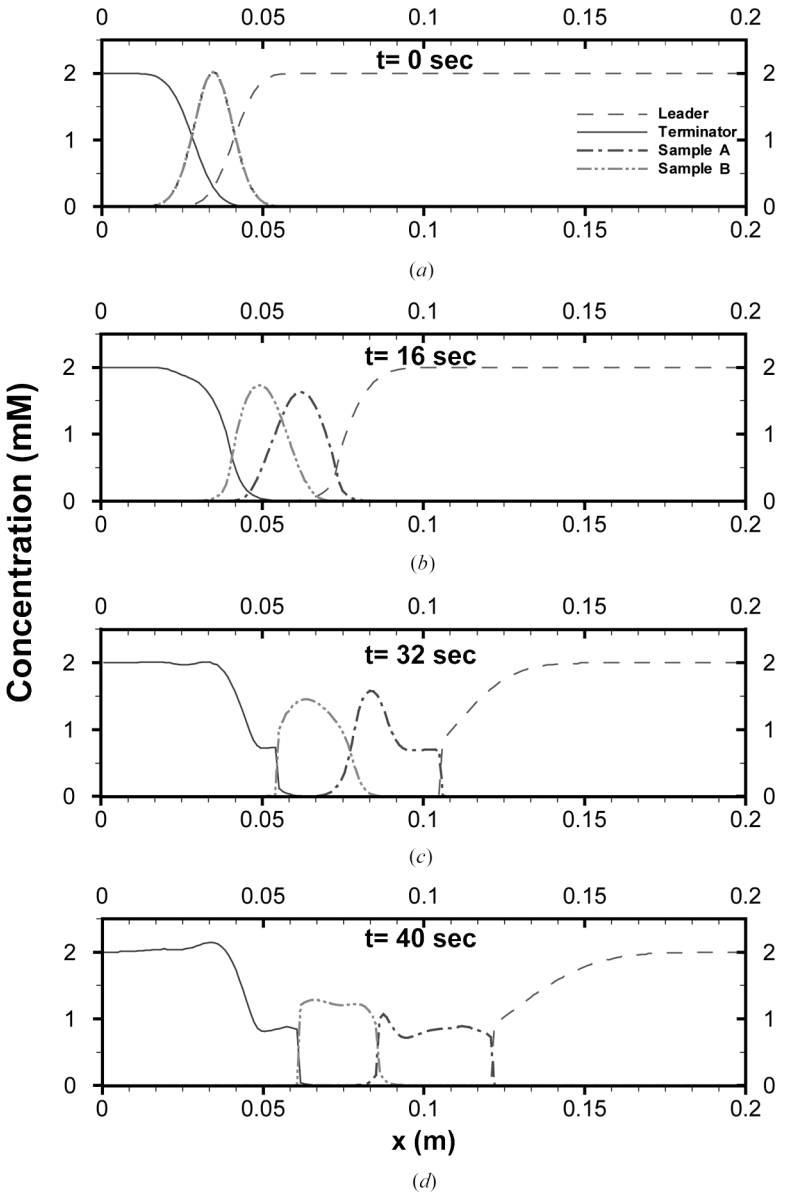

Figure 6. The transient behavior of all electrolytes in a planar microchannel. The power-law scheme is used in this ITP simulation for a nominal electric field of 300 V/cm. Input parameters and initial conditions are presented in Table 2 and Figure 3.

from sample B (Figure 6*b*). In the separation process (Figures 6*b* and 6*c*), the peak concentration of sample A is less than that of sample B. This is caused by the fact that the diffusion coefficient of sample A is higher than that of sample B due to the higher mobilities of sample A. Hence, sample A diffuses more in the transient

process. One would expect to have an identical peak height for sample A and sample B if the same diffusion coefficients were used for both samples.

As the separation continues, the leader creates a sharp boundary with sample A, while the terminator forms a steep interface with sample B (Figure 6*c*). In the meantime, samples A and B also keep on separating from each other, but they cannot form a distinct boundary like other electrolyte pairs. In other words, at 32 s an overlapping region between samples A and B still exists. This is because both sample A and sample B are well mixed initially, while other electrolyte pairs are quite separated at the beginning. Simulation results show that samples A and B create a steep boundary at 40 s, and all electrolytes continue to move toward the cathode. The discontinuous interfaces shown in the simulation are a hallmark of ITP separation [6–11]. The overlapping region between samples A and B can be minimized by running ITP at higher electric fields or by increasing the difference in electrophoretic mobilities between samples A and B. It is important to note that the ITP process presented here has not reached steady state. Steady-state ITP results can be obtained by running the simulation process for a longer time.

Figure 7 shows the conductivity distribution for the cases presented in Figure 6. The conductivity remains constant at the anodic and cathodic sides due to the uniform distribution of leader and terminator at the edges. The conductivity profile changes with the concentration distribution in the system. The sharp dips in the conductivity profiles are a signature of ITP boundary. The number of dips increases with the number of ITP boundary. There are two reasons for having the highest conductivity at the cathode ($x = 20$ cm). First, the cathodic side is always filled with leader. Second, the mobility of the leader is the highest in the ITP system considered here.

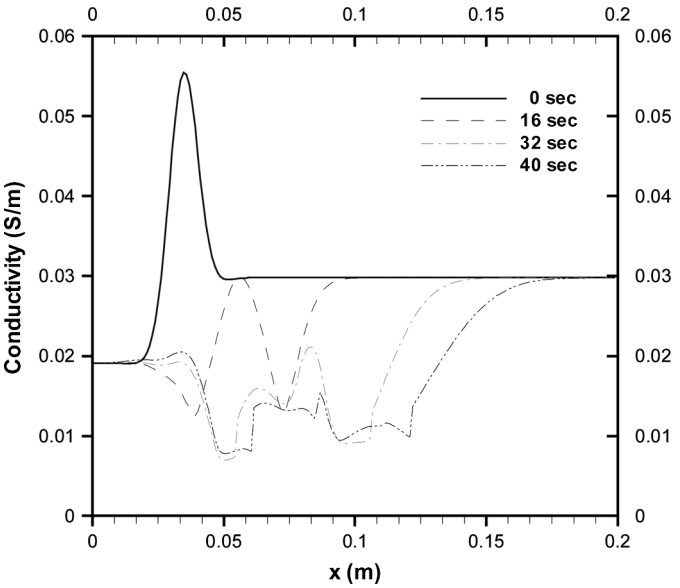

Figure 7. The transient conductivity profiles obtained from the power-law scheme. All conditions remain the same as for Figure 6.

4.4. Effects of Electric Potential

The effect of electric potential is very important in any electrokinetic phenomena. Simulations are performed to demonstrate the ITP behavior for three different electric field conditions. In all three cases, the cathodic side is maintained at ground (0 V), while the potentials at the anodic side is ranged between 4,000 and 6,000 V. The initial concentration distributions of all electrolytes are shown in Figure 3, and the mobilities and diffusion coefficients of each electrolyte are listed in Table 2. Figure 8 illustrates the concentration distribution of electrolytes (leader, sample A, sample B, and terminator) at 40 s after the initiation of the electric field. Two important features are immediately apparent in this figure: First, the electrophoretic velocity of electrolytes increases with the electric field, and the boundaries between neighboring electrolytes migrate toward the cathode as the electric field is increased. For instance, the boundaries between leader and sample A forms at $x = 12.1$ cm (Figure 8*c*) for a

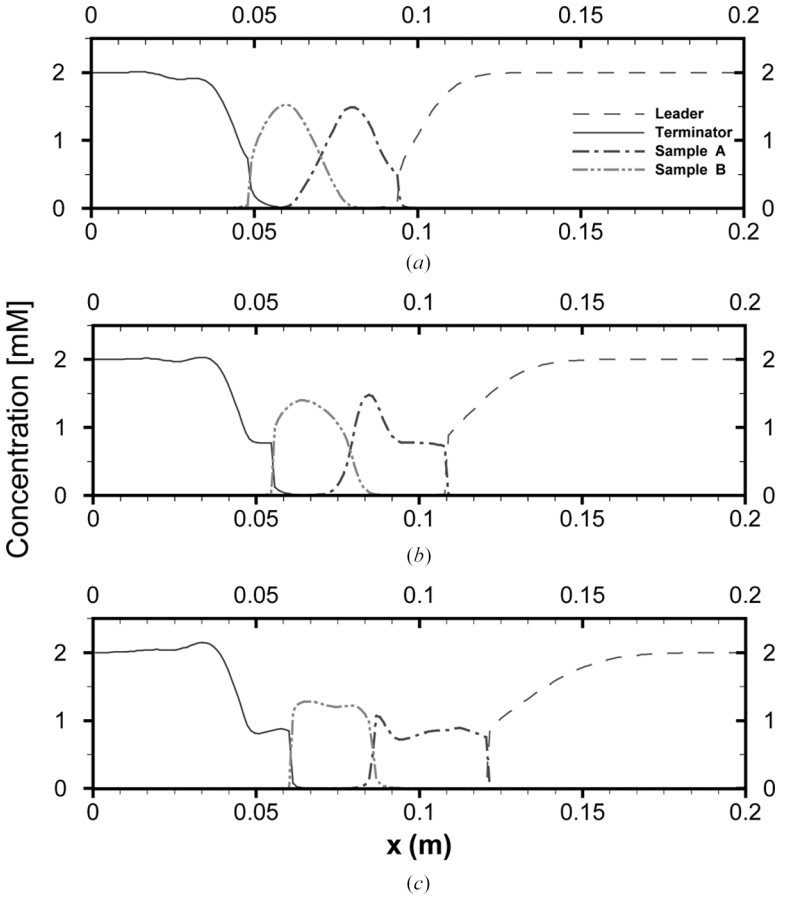

Figure 8. The effects of anodic voltage on the speed of ITP separation. Anodic voltages are (*a*) 4,000 V, (*b*) 5,000 V, and (*c*) 6,000 V, while the cathode is fixed to the ground. Numerical results are extracted at the channel centerline at 40 s.

nominal electric field of 300 V/cm, while this boundary is located at $x = 9.41$ cm (Figure 8*a*) and $x = 10.8$ cm (Figure 8*b*) for 200 V/cm and 250 V/cm, respectively. Second, the discrete boundaries between neighboring electrolytes form faster if the electric field increases. Figure 8 also demonstrates that the overlapping region between sample A and B decreases as the electric field increases.

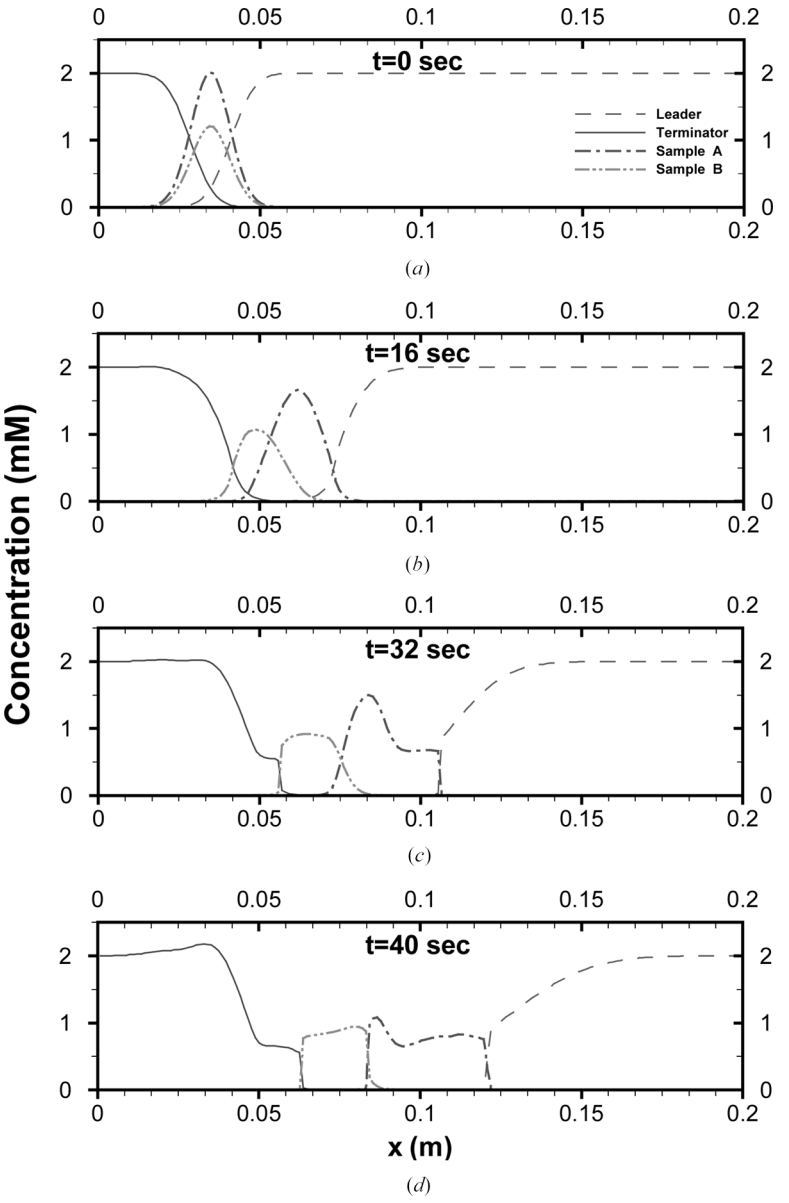

Figure 9. The transient behavior of all electrolytes in a planar microchannel for a nominal electric field of 300 V/cm. Numerical results are extracted at the channel centerline, and the power-law scheme is used in this ITP simulation. Input parameters are presented in Table 2.

4.5. Effects of Initial Concentration on Separation

System properties such as initial concentrations of samples and mobilities of electrolytes are of great importance to ITP separation, which can affect the movements of proteins or other ionic components in ITP separation process. The effect of samples' initial distribution is presented in this section. Figure 9 illustrates the transient behavior of an ITP train in a 2-D planar channel. The mobilities and diffusion coefficients of each electrolyte are presented in Table 2. The initial concentrations of the leader, terminator, sample A, and sample B are shown in Figure 9*a*. Note that the initial concentrations of all electrolytes are the same as for the case presented in Figure 6*a*, except for sample B. In this case the peak concentration of sample B is 60% less than that of Figure 6*a*. It is noteworthy to mention that the transient movements of sample A and sample B remain identical in Figure 6 and Figure 9 because the mobilities of sample A and sample B are assumed equal for both cases. At $t = 40$ s, the bandwidth of sample A remains almost identical in Figures 6 and 9. However, the bandwidth of sample B in Figure 9 (0.0209 m) is smaller than that in Figure 6 (0.0246 m), due to the mass differences in those cases. The peak concentration of sample B is significantly different in Figure 6 (1.28 mM) than that in Figure 9 (0.95 mM), also due to the mismatch in initial concentration.

5. SUMMARY AND CONCLUSIONS

Finite-volume schemes have been developed to simulate isotachophoresis in planar microchannels. ITP simulations have been performed for five ionic species: potassium ions (leader), tetrabutylammonium ions (terminator), sodium ions (sample A), tetraethylammonium ions (sample B), and chlorine ions (counterions). Upwind, hybrid, and power-law finite-volume schemes have been investigated for transient electromigration-diffusion problems. A normalized standard deviation has been introduced to find a suitable scheme for ITP simulation. According to the normalized standard deviation, the power-law scheme is superior to the others and the hybrid scheme is better than the upwind scheme. As in advection-diffusion problems, the power-law scheme is more expensive than any other method used here.

In order to obtain grid-independent results, ITP simulations have been carried out at different grid sizes. The numerical results reveal that cell Peclet number of 23 or less is appropriate for transient electromigration-diffusion problems using the power-law scheme. The critical cell Peclet number should be smaller for upwind and hybrid schemes. The effects of applied electric potential on the speed of an ITP separation have also been studied. The separation speed increases in proportion to the applied electric potential, but the applied potential does not significantly modify the transient behavior of the solutes in isotachophoresis. Finally, the samples' response to the initial input conditions was investigated. The simulation result, which was carried out using two different initial concentrations, showed that the initial concentration distribution plays a crucial role in the transient behavior of the samples.

REFERENCES

1. P. G. Righetti, C. J. van Oss, and J. W. Vanderhoff (eds.), *Electrokinetic Separation method*, Elsevier, Amsterdam, 1979.
2. J. Kendall and E. D. Crittenden, The Separation of Isotopes, *Proc. Natl. Acad. Sci. USA,* vol. 9, pp. 75–78, 1923.
3. F. M. Everaerts, J. L. Beckers, and T. P. E. M. Verheggen, *Isotachophoresis: Theory, Instrumentation and Applications*, Elsevier, Amsterdam, 1976.
4. H. Cui, P. Dutta, and C. F. Ivory, Isotachophoresis of Proteins in a Networked Microfluidic Chip: Experiment and 2D Simulation, *Electrophoresis*, vol. 28, pp. 1138–1145, 2007.
5. F. Kohlrausch, Über Concentrations-Verschiebungen durch Electrolyse im Inneren von Lösungen und Lösungsgemis, *Ann. Phys.*, vol. 62, pp. 209–220, 1897.
6. P. Boček, M. Deml, B. Kaplanová, and J. Janák, Analytical Isotachophoresis: The Concept of the Separation Capacity, *J. Chromatogr.*, vol. 160, pp. 1–9, 1978.
7. F. E. P. Mikkers, F. M. Everaerts, and J. A. F. Peek, Isotachophoresis: The Concepts of Resolution, Load Capacity and Separation Efficiency, *J. Chromatogr.*, vol. 168, pp. 293–315, 1979.
8. P. Gebauer, P. Boček, M. Deml, and J. Janák, Isotachophoresis of Kinetically Labile Complexes, *J. Chromatogr.*, vol. 199, pp. 81–94, 1980.
9. M. Bier, O. A. Palusinski, R. A. Mosher, and D. A. Saville, Electrophoresis: Mathematical Modeling and Computer Simulation, *Science*, vol. 219, pp. 1281–1297, 1983.
10. V. Fidler, J. Vacík, and Z. Fidler, Dynamics of Isotachophoretic Separation: Computer Simulation, *J. Chromatogr.*, vol. 320, pp. 167–174, 1985.
11. R. A. Mosher, D. A. Saville, and W. Thormann, *The Dynamics of Electrophoresis*, VCH, Weinheim, 1992.
12. J. Heinrich and H. Wagner, High Speed Electrophoresis Simulation for Optimization of Continuous Flow Electrophoresis and High Performance Capillary Techniques, *Electrophoresis*, vol. 13, pp. 44–49, 1992.
13. R. R. Deshmukh and M. Bier, Counterflow in Isotachophoresis: Computer Simulation and Experimental Studies, *Electrophoresis*, vol. 14, pp. 205–213, 1993.
14. K. Šlais, Model of Isotachophoresis (Displacement Electrophoresis) in Tapered Capillaries, *Electrophoresis*, vol. 16, pp. 2060–2068, 1995.
15. T. Hirokawa, H. Okamoto, and B. Gaš, High-sensitive Capillary Zone Electrophoresis Analysis by Electrokinetic Injection with Transient Isotachophoretic Preconcentration, *Electrophoresis*, vol. 24, pp. 498–504, 2003.
16. V. Hruška, M. Jaroš, and B. Gaš, Simul 5—Free Dynamic Simulator of Electrophoresis, *Electrophoresis*, vol. 27, pp. 984–991, 2006.
17. B. Jung, R. Bharadwaj, and J. G. Santiago, On-Chip Millionfold Sample Stacking Using Transient Isotachophoresis, *Anal. Chem.*, vol. 78, pp. 2319–2327, 2006.
18. H. Cui, K. Horiuchi, P. Dutta, and C. F. Ivory, Isoelectric Focusing in a Poly(dimethylsiloxane) Microfluidic Chip, *Anal. Chem.*, vol. 77, pp. 1303–1309, 2005.
19. W. Thormann and R. A. Mosher, Theoretical and Computer Aided Analysis of Steady State Moving Boundaries in Electrophoresis, *Transactions of the Society for Computer Simulation*, vol. 1, pp. 83–96, 1984.
20. P. S. Glockner and G. F. Naterer, Numerical Simulation of Electrokinetic Flow and Heat Transfer in Microchannels with a Finite-Volume Method, *Numer. Heat Transfer A*, vol. 49, pp. 451–470, 2006.
21. N. H. Saeid and Y. Yaacob, Natural Convection in a Square Cavity with Spatial Sidewall Temperature Variation, *Numer. Heat Transfer A*, vol. 49, pp. 683–697, 2006.

22. S. Sarkar, P. M. Raj, S. Chakraborty, and P. Dutta, Three-Dimensional Computational Modeling of Momentum, Heat, and Mass Transfer in a Laser Surface Alloying Process, *Numer. Heat Transfer A*, vol. 42, pp. 307–326, 2002.
23. A. Chatterjee, V. Prasad, and D. Sun, A Full 3-Dimensioal Adaptive Finite Volume Scheme for Transport and Phase-change Processes, *Numer. Heat Transfer A*, vol. 37, pp. 823–843, 2000.
24. P. Dutta, A. Beskok, and T. C. Warburton, Numerical Simulation of Mixed Electroosmotic/Pressure Driven Microflows, *Numer. Heat Transfer A*, vol. 41, pp. 131–148, 2002.
25. J. Shim, P. Dutta, and C. F. Ivory, Modeling and Simulation of Isoelectric Focusing in Two-Dimensional Microgeometries, *Electrophoresis*, vol. 28, pp. 572–586, 2007.
26. S. V. Patankar, *Numerical Heat Transfer and Fluid Flow*, Hemisphere, New York, 1980.